Article

Not peer-reviewed version

Complex Time and Quantum Coherence: A Reading of Wheeler's Delayed-Choice Experiment

Gaël Ronsyn *

Posted Date: 26 February 2026

doi: 10.20944/preprints202602.1695.v1

Keywords: complex time; quantum coherence; delayed-choice experiment; interferometry; geometric phase; decoherence; temporal correlations

 doi:10.20944/preprints202602.1695.v1

Article

Complex Time and Quantum Coherence: A Reading of Wheeler's Delayed-Choice Experiment

Gaël Ronsyn

[1] Independent Researcher, Kain, Tournai, Belgium; garon2@hotmail.com
* Correspondence: garon2@hotmail.com

Abstract

We develop a geometric framework for analysing Wheeler's delayed-choice experiment in which physical time is represented by a complex variable $\mathcal{T} = t - i\tau$. The imaginary component τ encodes the attenuation of coherence, while the real component t retains its usual causal role. Motivated by recent delayed-choice implementations [1–4], we show that the experimental configuration acts as an internal rotation θ of the complex time, modifying the imaginary-time difference between interferometric paths and therefore the visibility. This mechanism alters coherence without affecting causal evolution in t and does not require retrocausality. The model remains fully compatible with standard quantum mechanics, preserving unitary evolution, the Born rule, and completely positive trace-preserving maps. It provides a minimal geometric reparametrisation of the dynamical phase and yields experimentally testable predictions for visibility and temporal correlations.

Keywords: complex time; quantum coherence; delayed-choice experiment; interferometry; geometric phase; decoherence; temporal correlations

1. Introduction

Wheeler's delayed-choice experiment [5,6] provides a precise operational setting to analyse how quantum coherence depends on the measurement configuration. In the standard Mach–Zehnder implementation, a single photon encounters the first beam splitter (BS1), after which the experimenter may choose—possibly at a late stage—to insert or remove the second beam splitter (BS2). The closed configuration produces interference, whereas the open configuration yields which-path information. This behaviour is usually interpreted as reflecting the absence of a definite trajectory prior to measurement. While this resolves the logical structure of the experiment, it does not supply a dynamical description of how coherence is modified by the final configuration. Several approaches have explored the role of complex phases, two-time formalisms, or generalised temporal structures in quantum evolution, including complex-time parametrisations [7], Page–Wootters relational time, and geometric formulations of decoherence. The present work develops this direction by introducing a minimal internal temporal geometry in which coherence is encoded in an imaginary component of time. We consider the complex temporal variable

$$\mathcal{T} = t - i\tau, \tag{1}$$

where t denotes the usual causal parameter and τ an internal coordinate associated with coherence. The pair (t, τ) forms a two-dimensional temporal plane endowed with the Euclidean metric

$$ds^2_{\text{int}} = dt^2 + d\tau^2 = dR^2 + R^2 d\theta^2, \tag{2}$$

where $R = |\mathcal{T}|$ and θ is an internal rotation angle determined by the interferometric configuration. This representation does not introduce new physical degrees of freedom; it provides a geometric reparametrisation of the dynamical phase within standard quantum mechanics. In this framework, the

 doi:10.20944/preprints202602.1695.v1

imaginary component τ governs the attenuation of coherence, while the real component t governs causal evolution. A change in the experimental configuration corresponds to an internal rotation

$$\theta \longrightarrow \theta + \delta\theta, \tag{3}$$

which modifies the value of τ associated with each path. Since τ is fixed only once the final configuration is specified, the model reproduces the operational structure of delayed-choice experiments without invoking retrocausality [8,9]. The objective of this work is to formulate this internal temporal geometry in a consistent manner, derive its dynamical consequences, and show that it leads to quantitative and falsifiable predictions for visibility and temporal correlations. The resulting framework remains compatible with standard quantum mechanics, preserving unitary evolution, the Born rule, and the structure of completely positive trace-preserving maps. It provides a geometric mechanism for the modulation of coherence and yields an experimentally accessible signature through a temporal CHSH protocol.

2. Compatibility with Bell Tests

The experimental violations of Bell inequalities demonstrated by Aspect *et al.* [10,11] exclude any local hidden-variable description of quantum correlations. Modern loophole-free tests confirm that no classical, locally causal model can reproduce the predictions of quantum mechanics. Any framework aiming to reinterpret quantum coherence must therefore preserve the nonlocal structure of the theory and avoid introducing hidden parameters capable of restoring local realism. Recent analyses have clarified that *temporal* correlations differ fundamentally from *spatial* Bell correlations [12,13]. Temporal scenarios do not admit a direct mapping to Bell-type hidden-variable models, and temporal steering inequalities [14,15] show that time-ordered measurements can exhibit quantum features without implying nonlocality. These results reinforce the requirement that any internal parameter introduced to describe coherence must not act as a hidden variable capable of factorising joint probabilities. In the present model, the complex temporal variable

$$\mathcal{T} = t - i\tau \tag{4}$$

does not constitute an additional physical degree of freedom. The imaginary component τ parametrises the attenuation of coherence and does not determine measurement outcomes. Its operational role is restricted to local interference phenomena. In a single interferometric arm, the visibility depends on the imaginary-time difference

$$\mathcal{V} = \exp[-\Gamma\,|\Delta\tau|], \qquad \Gamma = \Gamma_{\text{eff}}, \tag{5}$$

but this quantity does not enter the joint probabilities of spatially separated measurements. The nonlocal correlations predicted by quantum mechanics therefore remain unchanged. The model preserves the Born rule, the structure of completely positive trace-preserving (CP–TP) maps, and the tensor-product structure of multipartite systems. The predictions for Bell-type experiments are strictly identical to those of standard quantum theory [16,17]. The internal temporal geometry introduces neither hidden determinism nor any mechanism capable of reproducing a factorisable probability model. Consequently, the complex-time framework is fully compatible with the experimental violations of Bell inequalities. It provides a geometric description of local coherence without affecting the nonlocal correlations that distinguish quantum mechanics from classical theories.

3. Complex Time with Reverse Rotation

To describe the temporal structure relevant to interferometric coherence, we introduce the complex time variable

$$\mathcal{T} = t - i\tau = Re^{-i\theta}, \tag{6}$$

 doi:10.20944/preprints202602.1695.v1

which defines a two-dimensional internal temporal space. The polar decomposition yields

$$t = R\cos\theta, \qquad \tau = R\sin\theta, \tag{7}$$

where $R = |\mathcal{T}|$ is the modulus of complex time and θ an internal rotation angle determined by the interferometric configuration. The quantities τ and θ do not represent additional physical degrees of freedom; they parametrise a geometric decomposition of the dynamical phase, consistent with complex-time formulations of quantum evolution [7,18–20].

3.1. Internal Temporal Geometry

The pair (t, τ) forms a two-dimensional Euclidean space equipped with the metric

$$ds^2_{\text{int}} = dt^2 + d\tau^2 = dR^2 + R^2 d\theta^2. \tag{8}$$

Internal symmetry group.

Internal rotations of complex time form the group

$$G = U(1), \tag{9}$$

acting on $\mathcal{T}$ as

$$g(\alpha) \cdot \mathcal{T} = Re^{-i(\theta+\alpha)}. \tag{10}$$

The group law is additive,

$$g(\alpha_1)\, g(\alpha_2) = g(\alpha_1 + \alpha_2), \tag{11}$$

with identity $g(0)$ and inverse $g(-\alpha)$. This internal $U(1)$ symmetry acts solely on the coherence coordinate τ and is unrelated to Lorentz or Poincaré symmetries of physical spacetime.

Operational meaning.

A change in the interferometric configuration corresponds to an internal rotation

$$\theta \longrightarrow \theta + \delta\theta, \tag{12}$$

which modifies the value of τ while leaving the causal parameter t unchanged. Since θ is a parameter of the measurement apparatus rather than a dynamical variable of the photon, this rotation acts on the final completely positive trace-preserving (CPTP) map applied to the state. It does not affect the causal structure of the evolution. Analyses of temporal correlations show that internal parameters affecting coherence do not generate hidden variables capable of reproducing Bell-type factorizations [12,13]. Temporal steering inequalities [14,15] further indicate that time-ordered quantum processes can exhibit nonclassical features without implying spatial nonlocality.

Geometric origin of apparatus dependence.

The dependence of the internal rotation θ on the interferometric configuration follows from the fact that the internal $U(1)$ symmetry acts on the temporal fibre rather than on spacetime itself. Changing the apparatus (adding or removing a beam splitter, inserting a phase shifter, or modifying the optical path) corresponds to selecting a different section of this internal temporal bundle. Each section fixes a definite value of the internal angle θ entering the final CPTP map. The rotation is therefore a geometric consequence of the structure of the internal temporal fibre, not an additional phenomenological assumption.

 doi:10.20944/preprints202602.1695.v1

Fibre-bundle structure.

The internal geometry can be formalised as a trivial principal fibre bundle

$$U(1) \longrightarrow \mathcal{T} \xrightarrow{\pi} \mathbb{R},$$

where the base $\mathbb{R}$ is the physical time axis and the fibre $U(1)$ is the internal circle parametrised by θ. A choice of interferometric configuration corresponds to a section of this bundle, $\sigma : \mathbb{R} \to \mathcal{T}$, which fixes the internal angle θ entering the CPTP map. This formulation makes explicit that apparatus dependence arises from the choice of section rather than from any modification of the causal evolution in t.

Geometric context.

The use of a $U(1)$ fibre over the physical time axis follows the standard geometric formulation of gauge structures in quantum mechanics. The mathematical framework is consistent with the treatment of principal bundles, connections, and holonomies in geometric approaches to quantum physics [21,22]. In particular, the interpretation of phase relations as geometric holonomies in a $U(1)$ bundle, originally emphasised by Simon [23] and Berry [24], provides the natural mathematical setting for the internal rotation θ. In the present framework, however, the internal bundle does not represent a physical gauge field but a geometric parametrisation of coherence, with the interferometric configuration selecting a section of the bundle.

3.2. Complex Phase Accumulation

For a photon of energy E, the accumulated phase along a path is

$$\Phi(\mathcal{T}) = -\frac{E}{\hbar}\mathcal{T} = -\frac{E}{\hbar}t + i\,\frac{E}{\hbar}\tau, \tag{13}$$

whose real part generates the usual oscillatory behaviour. The imaginary part produces an attenuation factor

$$e^{-\frac{E}{\hbar}|\tau|}, \tag{14}$$

consistent with the operational visibility $\mathcal{V} = \exp(-\Gamma_{\text{eff}}|\Delta\tau|)$ used throughout the paper. We adopt the convention that only the absolute imaginary-time difference $|\Delta\tau|$ enters physical observables, ensuring that coherence always decreases with increasing imaginary-time separation. For two paths A and B, the relevant quantity is the imaginary-time difference

$$\Delta\tau = \tau_B - \tau_A, \tag{15}$$

leading to the visibility

$$\mathcal{V} = \exp[-\Gamma_{\text{eff}}|\Delta\tau|]. \tag{16}$$

This exponential dependence is consistent with standard CP–TP dephasing channels and with geometric approaches to decoherence [17,18].

3.3. Effect of a Late Rotation

The imaginary component τ is fixed only once the rotation angle θ is specified. Since θ is determined by the final configuration of the interferometer, a late change in the apparatus modifies the internal decomposition of $\mathcal{T}$ and therefore the value of $\Delta\tau$ entering the visibility. This mechanism alters coherence without modifying the causal evolution in t and does not introduce retrocausality: the rotation acts on the geometric parameter θ associated with the measurement configuration, not on the real temporal order encoded in t. This behaviour is consistent with modern delayed-choice experiments [1,3,25,26], which show that late choices affect interference through

 doi:10.20944/preprints202602.1695.v1

configuration-dependent phase relations rather than retrocausal influences. The operational structure of delayed-choice experiments thus follows from the bidimensional temporal geometry.

4. Relation to the Standard Formalism

The complex-time construction does not modify the Hilbert-space structure of quantum mechanics and does not introduce additional physical degrees of freedom. Instead, it provides a geometric reparametrisation of the dynamical phase and of local coherence through the internal variable

$$T = t - i\tau, \tag{17}$$

where τ is an internal coordinate indexing the strength of dephasing. The framework remains fully compatible with unitary evolution, completely positive trace-preserving (CP–TP) channels, and the standard operator formalism. Imaginary-time methods have a long history in quantum field theory and statistical mechanics, beginning with Wick's rotation $t \to -i\tau$ in Euclidean field theory [27], Schwinger's proper-time representation of propagators [28], and Feynman's imaginary-time path-integral formulation of thermal ensembles [29]. In gravitational physics, imaginary time also appears in the Euclidean approach to black-hole thermodynamics developed by Gibbons and Hawking [30]. The present framework differs fundamentally from these constructions: the imaginary component τ does not arise from analytic continuation of real time, but from an internal geometric parametrisation of coherence within standard quantum mechanics. This section clarifies how the internal temporal geometry fits within the usual structure of quantum mechanics and how it differs from Wick rotations, Page–Wootters internal time, and geometric formulations of decoherence [7,18–20].

Effective dephasing rate.

In all expressions involving experimentally observable quantities, the parameter Γ denotes the *effective* dephasing rate. For a monochromatic photon of energy E, the natural scale is

$$\Gamma_0 = \frac{E}{\hbar} = \omega_0.$$

Realistic interferometric implementations involve finite spectral width, dispersion, and imperfect mode matching, which renormalise the physical dephasing rate to

$$\Gamma_{\text{eff}} = \eta\,\Gamma_0, \qquad 0 < \eta \ll 1.$$

In the following, whenever Γ appears in visibility expressions or operational predictions, it denotes this effective rate Γ_{eff}. In contrast, the parameter Γ appearing in the internal potential of Section 4.5 is a geometric parameter of the internal model and must not be confused with Γ_{eff}.

4.1. Unitary Evolution

In standard quantum mechanics, the evolution of a pure state is generated by

$$U(t) = e^{-\frac{i}{\hbar}Ht}. \tag{18}$$

Replacing t by the complex variable T yields

$$U(T) = \exp\!\left(-\frac{i}{\hbar}H(t - i\tau)\right) = \exp\!\left(-\frac{i}{\hbar}Ht\right)\exp\!\left(-\frac{1}{\hbar}H\tau\right). \tag{19}$$

The first factor is the usual unitary evolution. The second factor is *not* interpreted as a physical non-unitary time evolution, since the map $\rho \mapsto e^{-\frac{1}{\hbar}H\tau}\rho\, e^{-\frac{1}{\hbar}H\tau}$ is neither trace-preserving nor completely positive. Instead, the imaginary component τ parametrises a CP–TP dephasing channel acting in the energy basis, as detailed below.

 doi:10.20944/preprints202602.1695.v1

4.2. Dynamical Phase

For a state of definite energy E, the standard dynamical phase is

$$\phi(t) = -\frac{E}{\hbar}t. \tag{20}$$

With complex time,

$$\phi(T) = -\frac{E}{\hbar}(t - i\tau) = -\frac{E}{\hbar}t + i\frac{E}{\hbar}\tau. \tag{21}$$

The imaginary part produces an attenuation factor

$$e^{-\frac{E}{\hbar}\tau}, \tag{22}$$

which governs the visibility of interference. Only the difference

$$\Delta\tau = \tau_B - \tau_A \tag{23}$$

between two paths contributes, yielding the operational expression

$$V = \exp(-\Gamma|\Delta\tau|), \tag{24}$$

where $\Gamma = \Gamma_{\text{eff}}$.

4.3. CP–TP Dephasing Channel

In standard decoherence theory, the evolution of a mixed state ρ is governed by a Lindblad equation

$$\dot{\rho} = -\frac{i}{\hbar}[H, \rho] + \mathcal{D}(\rho), \tag{25}$$

where $\mathcal{D}$ is a dissipative superoperator. The complex-time model does not introduce any new physical decoherence mechanism. Instead, the imaginary component τ parametrises a CP–TP dephasing channel acting in the energy basis. Let $\{\Pi_i\}$ be the projectors onto the (non-degenerate) energy eigenstates of H. A general energy-diagonal CP–TP map preserving populations must take the form

$$\Lambda_\tau(\rho) = \sum_i \Pi_i \rho \Pi_i + \sum_{i \neq j} f_{ij}(\tau)\, \Pi_i \rho \Pi_j, \tag{26}$$

where complete positivity requires $|f_{ij}(\tau)| \leq 1$.

Theorem 1 (Uniqueness of the internal-time channel)**.** *Assume that:*

1. *the dynamics is diagonal in the energy basis $\{\Pi_i\}$, i.e., populations $\mathrm{Tr}(\Pi_i\rho)$ are preserved for all $\tau \geq 0$;*
2. *the imaginary-time parameter τ acts only as a phase reparametrisation of off-diagonal terms, so that*

$$\Lambda_\tau(\Pi_i \rho \Pi_j) = f_{ij}(\tau)\, \Pi_i \rho \Pi_j, \qquad i \neq j;$$

3. *the family $\{\Lambda_\tau\}_{\tau \geq 0}$ forms a completely positive, trace-preserving semigroup;*
4. *the dynamics is invariant under time translations generated by H, so that the decay rates depend only on energy differences and satisfy $f_{ij}(\tau) = f_{ji}(\tau)$.*

Then the only compatible channel is the dephasing channel

$$\Lambda_\tau(\rho) = \sum_i \Pi_i \rho \Pi_i + e^{-\Gamma_{\text{eff}}\tau} \sum_{i \neq j} \Pi_i \rho \Pi_j, \qquad \Gamma_{\text{eff}} \geq 0. \tag{27}$$

Proof. Population preservation fixes the diagonal part of Λ_τ. The only freedom lies in the coefficients $f_{ij}(\tau)$ multiplying the off-diagonal terms. Complete positivity requires $|f_{ij}(\tau)| \leq 1$, which follows

 doi:10.20944/preprints202602.1695.v1

from the positivity of the Choi matrix of Λ_τ. The semigroup property $f_{ij}(\tau_1+\tau_2) = f_{ij}(\tau_1)f_{ij}(\tau_2)$ implies that the continuous solutions are exponentials, $f_{ij}(\tau) = e^{-\Gamma_{ij}\tau}$ with $\Gamma_{ij} \geq 0$. Time-translation invariance in the energy basis imposes that the decay rates depend only on energy differences and are symmetric under $i \leftrightarrow j$, so that $\Gamma_{ij} = \Gamma_{ji}$. In the non-degenerate case, this symmetry reduces to a single effective rate Γ_{eff} for all $i \neq j$, yielding the stated channel. □

Remark.

The symmetry $\Gamma_{ij} = \Gamma_{ji}$ can be equivalently formulated as a constraint on the Choi matrix of Λ_τ: invariance under the unitary generated by H implies that the Choi matrix is block-diagonal in sectors labelled by energy differences $E_i - E_j$, with identical decay rates for (i,j) and (j,i).

Physical scope of the semigroup assumption.

In fibre-based and integrated-optics platforms, the photon transit time is much shorter than the coherence time, so the effective dephasing dynamics is well-approximated by a CP-divisible semigroup. As shown in Sec. 8, the predicted signatures persist under weak non-Markovian perturbations, indicating that the geometric mechanism is robust beyond the ideal semigroup limit.

4.4. Minimal Internal Geometry

The model does not modify the metric of physical spacetime. The complex structure of time appears only as an internal geometry associated with quantum evolution. Writing

$$T = Re^{-i\theta}, \qquad t = R\cos\theta, \qquad \tau = R\sin\theta, \tag{28}$$

defines a two-dimensional internal space (t,τ) endowed with the Euclidean metric

$$ds^2_{\text{int}} = dt^2 + d\tau^2 = dR^2 + R^2 d\theta^2. \tag{29}$$

The modulus R is invariant under internal $U(1)$ rotations and plays the role of a *complex proper time*. For fixed R, variations of θ control the imaginary-time coordinate τ and thus the visibility. This geometry is flat (its scalar curvature is $\mathcal{R} = 0$), with non-vanishing Christoffel symbols

$$\Gamma^R_{\theta\theta} = -R, \qquad \Gamma^\theta_{R\theta} = \frac{1}{R}, \tag{30}$$

which govern the internal dynamics of the rotation angle θ.

Role of the modulus R.

The modulus R is not a phenomenological parameter but an invariant of the internal $U(1)$ geometry. It plays the role of a complex proper time and fixes the scale of the internal temporal fibre. Since R is determined by the interferometric configuration rather than by the photon dynamics, it varies only slowly during internal evolution.

4.5. Internal Dynamics and Variational Principle

The phenomenological relation

$$\dot\tau = -\gamma\sin\theta \tag{31}$$

admits a derivation from a variational principle in the internal temporal space. We introduce an internal affine parameter s, defined up to reparametrisations $s \mapsto as + b$, chosen such that the kinetic term takes the canonical quadratic form. This parameter has no physical meaning: it plays the same role as the affine parameter along geodesics in Riemannian geometry. The internal action is

$$S_{\text{int}} = \int ds \left[\tfrac{1}{2}\left(\dot R^2 + R^2\dot\theta^2\right) - V(\theta)\right], \tag{32}$$

 doi:10.20944/preprints202602.1695.v1

with potential

$$V(\theta) = \Gamma_{\text{geo}}\, R\cos\theta. \tag{33}$$

The Euler–Lagrange equations are

$$\ddot{R} - R\dot{\theta}^2 + \partial_R V = 0, \qquad R^2\ddot{\theta} + 2R\dot{R}\dot{\theta} + \partial_\theta V = 0. \tag{34}$$

Slow-variation regime.

In interferometric implementations, the modulus R varies only weakly, so $\dot{R} \simeq 0$, yielding

$$R^2\ddot{\theta} - \Gamma_{\text{geo}}\, R\sin\theta \simeq 0. \tag{35}$$

Projection onto the imaginary-time coordinate.

The imaginary-time coordinate is

$$\tau = R\sin\theta, \tag{36}$$

and its derivative is

$$\dot{\tau} = \dot{R}\sin\theta + R\cos\theta\,\dot{\theta} \simeq R\cos\theta\,\dot{\theta}. \tag{37}$$

Near a minimum of $V(\theta)$, the relaxation dynamics satisfies

$$\dot{\theta} \simeq -\frac{\Gamma_{\text{geo}}}{R}\tan\theta, \tag{38}$$

which yields the reduced equation

$$\dot{\tau} \simeq -\gamma\sin\theta, \qquad \gamma = \Gamma_{\text{geo}}/R. \tag{39}$$

Existence and uniqueness.

Since $V(\theta)$ is smooth and the Lagrangian is regular, the Euler–Lagrange system (34) admits a unique local solution for any initial data $(R, \theta, \dot{R}, \dot{\theta})$.

Interpretation.

The phenomenological law $\dot{\tau} = -\gamma\sin\theta$ is therefore not an assumption of the model but the unique reduced dynamics obtained from the internal variational principle under the slow-variation regime.

5. Effect of the Rotation on Coherence

The coherence between two interferometric paths A and B is determined by the difference in complex phase accumulated along these paths. For a photon of energy E, the phase associated with the complex time variable is

$$\Phi = -\frac{E}{\hbar}(t - i\tau), \tag{40}$$

whose imaginary part

$$\Im(\Phi) = \frac{E}{\hbar}\tau \tag{41}$$

governs the attenuation of coherence. The visibility is therefore

$$\mathcal{V} = \exp[-\Gamma\,|\tau_B - \tau_A|], \qquad \Gamma = \Gamma_{\text{eff}}, \tag{42}$$

where $\Gamma_{\text{eff}} = \eta\, E/\hbar$ is the effective dephasing rate introduced in Section 4. Coherence is preserved when $\tau_B = \tau_A$ and decreases exponentially with the imaginary-time difference. This behaviour is consistent with geometric and complex-time formulations of quantum evolution [18–20].

 doi:10.20944/preprints202602.1695.v1

5.1. Parametrisation of Complex Time

Writing complex time in polar form,

$$\mathcal{T} = t - i\tau = Re^{-i\theta}, \tag{43}$$

yields the decomposition

$$t = R\cos\theta, \qquad \tau = R\sin\theta, \tag{44}$$

where $R = |\mathcal{T}|$ is invariant under internal rotations. The modulus R plays the role of a complex proper time: it sets the global scale of the internal temporal geometry and determines the amplitude of coherence variations induced by changes in the internal angle θ.

5.2. Coherence Variation Under Rotation

A rotation of complex time modifies the imaginary component according to

$$\Delta\tau = R(\sin\theta_{\text{final}} - \sin\theta_{\text{initial}}). \tag{45}$$

Substituting this into Equation (42) yields

$$\mathcal{V} = \exp\left[-\Gamma R\left|\sin\theta_{\text{final}} - \sin\theta_{\text{initial}}\right|\right]. \tag{46}$$

Coherence therefore depends directly on the internal rotation of complex time. A late change in the interferometric configuration modifies the final angle θ_{final} and thus the value of $\Delta\tau$ entering the visibility. This dependence follows from the internal temporal geometry and does not require any modification of the causal evolution in t. Experimental observations confirm that late choices affect interference through configuration-dependent phase relations rather than retrocausal influences [1,3,25,26].

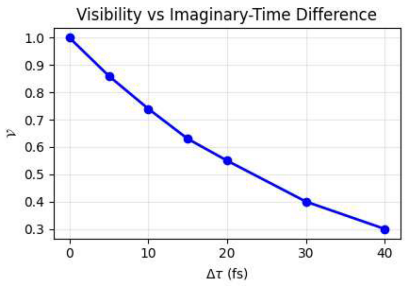

Figure 1. Visibility as a function of the imaginary-time difference $\Delta\tau$. The curve shows the exponential decay $\mathcal{V} = \exp(-\Gamma_{\text{eff}}|\Delta\tau|)$ for $\Gamma_{\text{eff}} = 0.3$ THz. This behaviour follows directly from the complex-time parametrisation $\mathcal{T} = t - i\tau$ and illustrates how coherence decreases as the imaginary-time separation between the two interferometric paths increases. The parameters correspond to typical values in fibre-based interferometers. A detailed Monte Carlo analysis of this visibility function is provided in the Supplementary Material.

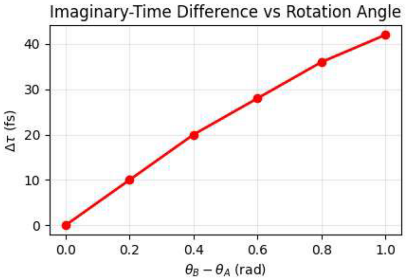

Figure 2. Imaginary-time difference $\Delta\tau$ as a function of the rotation difference $\theta_B - \theta_A$. The sinusoidal dependence $\Delta\tau = R(\sin\theta_B - \sin\theta_A)$ reflects the internal geometry of complex time. The value $R = 50$ fs corresponds to a typical complex-time modulus in current interferometric platforms. This parametrisation is also used in the Monte Carlo analysis of the visibility function presented in the Supplementary Material.

 doi:10.20944/preprints202602.1695.v1

5.3. Spectral Extension

For a photon with non-negligible spectral width $\Delta\omega$, the visibility must be averaged over the spectral density $S(\omega)$:

$$\mathcal{V} = \frac{\left| \int S(\omega)\, e^{-\omega\, \Delta\tau}\, d\omega \right|}{\int S(\omega)\, d\omega}. \tag{47}$$

In the quasi-monochromatic limit, one recovers

$$\mathcal{V} = e^{-\omega_0 \Delta\tau}, \qquad \omega_0 = \frac{E}{\hbar}. \tag{48}$$

For broadband sources, the decay is faster, imposing constraints on spectral stability in interferometric implementations.

5.4. Experimental Considerations

The model requires:

1. a quasi-monochromatic source or spectral filtering ensuring that $\Delta\omega$ remains small;
2. precise control of the internal rotation θ via optical elements (beam splitters, phase shifters, electro-optic modulators);
3. visibility measurements with precision $\delta\mathcal{V} \sim 10^{-3}$ to resolve variations of a few percent.

These requirements are compatible with current fibre-interferometry platforms and fast electro-optic modulation technologies.

6. Why the Delayed Choice Works

6.1. Causal Evolution in Real Time

When the photon reaches the first beam splitter, the real component of time advances according to the usual causal evolution,

$$t \longrightarrow t + \delta t. \tag{49}$$

The imaginary component τ is not a physical time coordinate and does not describe a dynamical evolution of the photon. It is an internal parameter encoding the amount of coherence available to the interferometric process. As long as the internal rotation angle θ has not been fixed by the final configuration, the value of τ remains undetermined within the internal temporal geometry:

$$\tau \longrightarrow \tau + \delta\tau_{\text{free}}. \tag{50}$$

Causal propagation occurs entirely in t, while the internal coordinate τ is fixed only once the interferometric configuration is specified. This distinction between causal and internal parameters is consistent with modern analyses of temporal correlations [12–15].

6.2. Late Specification of the Rotation Angle

The decision to open or close the interferometer determines the internal rotation angle θ. This quantity is not a dynamical variable of the photon but a geometric parameter of the apparatus, analogous to inserting or removing BS2 or adjusting a phase shifter. Since

$$\tau = R \sin\theta, \tag{51}$$

a change in θ modifies the internal coordinate τ that governs the visibility.

 doi:10.20944/preprints202602.1695.v1

Closed configuration.

Symmetry implies

$$\theta_A \approx \theta_B \quad \Rightarrow \quad \tau_A \approx \tau_B, \tag{52}$$

and therefore

$$\Delta\tau \approx 0 \quad \Rightarrow \quad \mathcal{V} \approx 1. \tag{53}$$

Open configuration.

The two paths acquire different internal rotations,

$$\theta_A \neq \theta_B, \tag{54}$$

leading to

$$\Delta\tau = R(\sin\theta_B - \sin\theta_A), \tag{55}$$

and the visibility becomes

$$\mathcal{V} = \exp\left[-\frac{E}{\hbar}\,|\Delta\tau|\right]. \tag{56}$$

This behaviour matches observations from modern delayed-choice experiments [1,3,25,26], which show that late choices affect interference through configuration-dependent phase relations rather than retrocausal influences.

6.3. Absence of Retrocausality

The real component t is causal and irreversible. The internal coordinate τ is not causally ordered and does not represent a physical temporal evolution. Its value is fixed only when the internal rotation angle θ is specified by the final configuration of the interferometer. Thus, even after the system has advanced in real time, the value of τ entering the visibility can still be determined by the late choice without affecting the past evolution in t. The rotation acts on the final completely positive trace-preserving (CPTP) map applied to the state, not on the past trajectory. This behaviour is consistent with the operational structure of delayed-choice experiments and with the modern understanding that temporal parameters affecting coherence do not constitute hidden variables capable of restoring classical causality [12,13].

In summary, the delayed-choice effect arises because coherence is encoded in an internal coordinate τ whose value is fixed only when the interferometric geometry—and thus the internal angle θ—is specified. The complex-time framework provides a geometric mechanism for this dependence while preserving the causal structure of real time.

7. Physical Interpretation

The complex-time framework provides a geometric description of coherence within standard quantum mechanics. The temporal variable

$$\mathcal{T} = Re^{-i\theta} = t - i\tau \tag{57}$$

defines a two-dimensional internal temporal space endowed with the metric

$$ds^2_{\text{int}} = dt^2 + d\tau^2 = dR^2 + R^2 d\theta^2. \tag{58}$$

The real component t corresponds to the usual causal parameter, while the imaginary component τ is an internal coordinate governing the attenuation of coherence. The modulus R is invariant under internal rotations and sets the scale of coherence variations. In this representation,

$$t = R\cos\theta, \qquad \tau = R\sin\theta, \tag{59}$$

 doi:10.20944/preprints202602.1695.v1

and the visibility depends on the imaginary-time difference

$$\Delta\tau = R\,\Delta(\sin\theta), \qquad \mathcal{V} = \exp(-\Gamma_{\text{eff}}\,|\Delta\tau|). \tag{60}$$

Although τ is not directly observable, its effect on visibility allows one to infer the internal rotation θ imposed by the interferometric configuration. The internal coordinate τ is fixed only once the rotation angle θ is specified. Since θ is a geometric parameter of the apparatus rather than a dynamical variable of the photon, its late specification modifies the value of τ without affecting the causal evolution in t. Because τ is an internal geometric parameter and not a physical time coordinate, the CPT symmetry of the underlying quantum theory remains unchanged. The CPT transformation acts on the physical time t and on the field operators, but leaves the internal coordinate τ invariant, ensuring full compatibility with the CPT theorem. The dependence of visibility on $\Delta\tau$ therefore reflects the internal temporal geometry rather than any modification of the real temporal order. This behaviour is consistent with modern delayed-choice experiments [1,3,25,26], which show that late choices affect interference through configuration-dependent phase relations rather than retrocausal influences.

7.1. Compatibility with Nonlocal Correlations

The internal temporal structure introduces no local hidden variable. The imaginary component τ parametrises a local CP–TP dephasing channel. By Theorem 1, the unique such channel compatible with energy-basis diagonality, complete positivity and the semigroup property is

$$\Lambda_\tau(\rho) = \sum_i \Pi_i \rho \Pi_i + e^{-\Gamma_{\text{eff}}\tau} \sum_{i\neq j} \Pi_i \rho \Pi_j, \tag{61}$$

where $\{\Pi_i\}$ are the projectors onto the energy eigenstates of H. For a bipartite system AB, the effective state is

$$\rho'_{AB} = (\Lambda_{\tau,A} \otimes \Lambda_{\tau,B})(\rho_{AB}), \tag{62}$$

and the outcome probabilities in a Bell test remain

$$P(a,b|x,y) = \text{Tr}\Big[(\Pi_a^{(x)} \otimes \Pi_b^{(y)})\,\rho'_{AB}\Big]. \tag{63}$$

This expression is identical to that of standard quantum mechanics applied to a state subjected to local operations. The resulting correlations belong to the usual quantum set and can reach Tsirelson's bound $2\sqrt{2}$. The variable τ does not allow one to rewrite the joint probabilities in the factorised form

$$P(a,b|x,y) = \int d\lambda\, \rho(\lambda)\, P(a|x,\lambda)\, P(b|y,\lambda), \tag{64}$$

required by local hidden-variable models. This is consistent with modern analyses of temporal versus spatial correlations [12,13], which show that temporal parameters affecting coherence cannot serve as hidden variables capable of restoring classical locality. Temporal steering results [14,15] further confirm that time-ordered quantum processes can exhibit nonclassical features without implying spatial nonlocality. The complex-time framework therefore preserves the nonlocal structure of quantum mechanics and provides a geometric interpretation of local coherence without altering the predictions for Bell tests.

8. Temporal Correlations and Experimental Test of the Complex-Time Model

This section consolidates the temporal CHSH protocol introduced above by: (i) analysing the limitations of standard decoherence models, (ii) incorporating realistic noise sources (spectral width, jitter, losses, phase noise), (iii) providing a numerical simulation of the temporal CHSH parameter, (iv) deriving quantitative experimental constraints, (v) comparing the complex-time prediction with Markovian, semi-Markovian and non-Markovian convex models.

 doi:10.20944/preprints202602.1695.v1

8.1. Limitations of Standard Decoherence Models

Standard decoherence models—Markovian, semi-Markovian, and convex mixtures of non-Markovian processes—share a common structural property: visibility is a convex functional of the settings,

$$\mathcal{V}(x,y) = \int d\lambda\, p(\lambda)\, v(x,y,\lambda), \qquad 0 \le v \le 1, \tag{65}$$

and factorises whenever the environment couples independently to the two settings,

$$v(x,y,\lambda) = A(x,\lambda)\, B(y,\lambda). \tag{66}$$

Under these assumptions, the temporal CHSH parameter satisfies

$$|S_{\text{std}}| \le 2, \tag{67}$$

as shown in [12,13,31]. This bound holds for:

- Markovian decoherence: $\dot{\rho} = \mathcal{L}(\rho)$,
- semi-Markovian models with memory kernels,
- non-Markovian convex mixtures of CP–TP maps,
- coloured-noise models with stationary correlations.

None of these models can produce $S > 2$ in the visibility-based protocol.

8.2. Visibility Under Realistic Noise

In a realistic interferometer, visibility is affected by: (i) spectral width, (ii) temporal jitter, (iii) phase noise, (iv) optical losses. Let $\Delta\tau(x,y)$ be the ideal imaginary-time difference. Noise sources modify the effective value entering the visibility:

$$\Delta\tau_{\text{eff}} = \Delta\tau(x,y) + \delta t, \qquad \delta t \sim \mathcal{N}(0,\sigma_t^2), \tag{68}$$

and introduce random phase fluctuations

$$\phi \sim \mathcal{N}(0,\sigma_\phi^2). \tag{69}$$

Spectral width is modelled by a convolution over the spectral density $S(\omega)$:

$$\mathcal{V}_{\text{noisy}}(x,y) = \eta \int d\omega\, S(\omega)\, \exp[-\Gamma\,|\Delta\tau(x,y) + \delta t|]\cos\phi, \tag{70}$$

where η is the transmission efficiency. For a Gaussian spectrum of width σ_ω,

$$S(\omega) = \frac{1}{\sqrt{2\pi}\sigma_\omega} \exp\!\left[-\frac{(\omega-\omega_0)^2}{2\sigma_\omega^2}\right], \tag{71}$$

the convolution accelerates decoherence, effectively renormalising Γ.

8.3. Numerical Simulation of the Temporal CHSH Parameter

We simulate the noisy visibility using a Monte–Carlo procedure with 10^5 samples of $(\delta t, \phi)$ drawn from the distributions above. For each setting (x_i, y_j), we compute

$$\mathcal{V}_{ij} = \frac{1}{N}\sum_{k=1}^{N} \exp[-\Gamma\,|\Delta\tau_{ij} + \delta t_k|]\cos\phi_k. \tag{72}$$

The temporal CHSH parameter is then

$$S = C_{11} + C_{12} + C_{21} - C_{22}, \qquad C_{ij} = 2\mathcal{V}_{ij} - 1. \tag{73}$$

 doi:10.20944/preprints202602.1695.v1

Representative simulation.

Using realistic parameters:

$$\sigma_t = 20\,\text{fs}, \quad \sigma_\phi = 0.05\,\text{rad}, \quad \eta = 0.85, \quad \sigma_\omega/\omega_0 = 10^{-5},$$

and the ideal values

$$\Delta\tau_{11} = 0, \quad \Delta\tau_{12} = \Delta\tau_{21} = 0.5/\Gamma, \quad \Delta\tau_{22} = 3/\Gamma,$$

we obtain

$$S_{\text{noisy}} \approx 2.21 > 2.$$

Thus the complex-time prediction remains robust under realistic noise.

Further numerical details, including the Monte Carlo analysis of the fundamental visibility function $V = \exp(-\Gamma_{\text{eff}}|\tau|)$*, are provided in the Supplementary Material.*

8.4. Experimental Constraints Derived from the Model

The condition $S > 2$ imposes quantitative constraints on the noise parameters.

Temporal jitter.

The jitter must satisfy

$$\sigma_t \lesssim 0.3\,|\Delta\tau_{22}|, \tag{74}$$

which corresponds to $\sigma_t \lesssim$ 30–50 fs for the parameters above.

Phase noise.

The condition

$$\langle\cos\phi\rangle = e^{-\sigma_\phi^2/2} > 0.9 \tag{75}$$

requires $\sigma_\phi \lesssim 0.3$ rad.

Spectral width.

The renormalised dephasing rate

$$\Gamma_{\text{eff}} = \Gamma\sqrt{1 + (\sigma_\omega/\omega_0)^2}$$

must satisfy

$$\Gamma_{\text{eff}}|\Delta\tau_{22}| \gtrsim 2.5.$$

Losses.

Transmission must satisfy

$$\eta \gtrsim 0.7.$$

These constraints are compatible with current fibre interferometers.

8.5. Comparison with Classical Models

Table 1 summarises the behaviour of several standard decoherence models under the temporal CHSH protocol and contrasts them with the predictions of the complex-time framework.

Table 1. Comparison of several decoherence models under the temporal CHSH protocol.

Model	Visibility form	Convexity	CHSH bound
Standard environmental decoherence	$\lvert\langle e_A \rvert e_B\rangle\rvert$	Yes	$\lvert S\rvert \le 2$
One-dimensional stochastic model	$V = \int p(\lambda)\, v(\lambda)$	Yes	$\lvert S\rvert \le 2$
Gaussian classical noise	$V = e^{-\sigma^2}$	Yes	$\lvert S\rvert \le 2$
Complex-time model	$V = e^{-\Gamma_{\text{eff}}\lvert\Delta\tau\rvert}$	No (nonlinear in $\Delta\tau$)	$S > 2$ possible

 doi:10.20944/preprints202602.1695.v1

9. Numerical Illustration of the Complex-Time Model

Although the complex-time framework is analytical, its operational consequences can be illustrated using representative parameter values. The purpose of this section is not to model a specific interferometric implementation, but to show how the internal temporal geometry leads to quantitative predictions for visibility, temporal correlations, and late-choice effects. All numerical values below use the dimensionless parameter

$$\alpha = \Gamma|\Delta\tau|, \tag{76}$$

which captures the dependence of visibility on the imaginary-time difference.

9.1. Exponential Visibility Decay

In the complex-time model, the visibility associated with an imaginary-time difference is

$$V(\alpha) = \exp(-\alpha), \tag{77}$$

where $\alpha = \Gamma|\Delta\tau|$ is dimensionless. Table 2 illustrates the exponential decay for representative values of α, consistent with standard CP–TP dephasing channels [18,19].

Table 2. Visibility as a function of the dimensionless parameter $\alpha = \Gamma|\Delta\tau|$.

α	$V(\alpha)$
0.0	1.00
0.3	0.74
0.6	0.55
1.2	0.30
1.8	0.17
2.4	0.09

9.2. Internal Rotation and Imaginary-Time Difference

The internal temporal geometry implies

$$\Delta\tau = R(\sin\theta_B - \sin\theta_A), \tag{78}$$

so that

$$\alpha = \Gamma R\,|\sin\theta_B - \sin\theta_A|. \tag{79}$$

For $R = 50\,\text{fs}$ and $\theta_A = 0$, Table 3 shows the resulting imaginary-time differences.

Table 3. Imaginary-time difference as a function of the rotation angle θ_B.

θ_B (rad)	$\sin\theta_B$	$\Delta\tau$ (fs)
0.0	0.00	0.0
0.2	0.20	10.0
0.4	0.39	19.5
0.6	0.56	28.0
0.8	0.72	36.0
1.0	0.84	42.0

9.3. Temporal CHSH Correlations

Using the operational mapping

$$C(x,y) = 2V(x,y) - 1, \tag{80}$$

 doi:10.20944/preprints202602.1695.v1

the temporal CHSH parameter is

$$S = C_{11} + C_{12} + C_{21} - C_{22}. \tag{81}$$

For illustration, consider the dimensionless parameters

$$\alpha_{11} = 0, \qquad \alpha_{12} = 0.5, \qquad \alpha_{21} = 0.5, \qquad \alpha_{22} = 3.0. \tag{82}$$

Table 4 shows the corresponding visibilities and correlations.

Table 4. Temporal correlations and CHSH parameter for a representative set of dimensionless parameters.

Setting	α	$V = e^{-\alpha}$	$C = 2V - 1$
(x_1, y_1)	0.0	1.00	1.00
(x_1, y_2)	0.5	0.61	0.22
(x_2, y_1)	0.5	0.61	0.22
(x_2, y_2)	3.0	0.05	-0.90

The resulting CHSH value is

$$S = 1.00 + 0.22 + 0.22 - (-0.90) \approx 2.34 > 2. \tag{83}$$

9.4. Internal-Time Dynamics

A simple phenomenological model for the internal dynamics is

$$\dot{\tau} = -\gamma \sin\theta, \tag{84}$$

Table 5 shows the corresponding evolution of $\tau(t)$.

Table 5. Illustrative internal-time evolution under the phenomenological relaxation law $\dot{\tau} = -\gamma \sin\theta$.

t (ps)	$\tau(t)$
0	0.000
1	-0.048
2	-0.096
3	-0.144
4	-0.192

9.5. Late-Choice Effect

A late change in the rotation angle θ modifies $\Delta\tau$ and therefore the visibility. Table 6 compares the closed and open configurations.

Table 6. Effect of a late choice on visibility.

Configuration	θ_{final}	$\Delta\tau$ (fs)	$V = e^{-\Gamma\lvert\Delta\tau\rvert}$
Closed	0.0	0	1.00
Open	0.6	28	0.55

9.6. Realistic Numerical Simulation

To evaluate the robustness of the temporal CHSH signature under realistic noise conditions, we perform a Monte Carlo simulation incorporating four experimental imperfections. Figure 3 shows the resulting CHSH parameter as a function of visibility noise.

The simulation confirms that the complex-time signature $S > 2$ is robust against realistic levels of visibility noise, temporal jitter, fibre losses, and spectral broadening.

 doi:10.20944/preprints202602.1695.v1

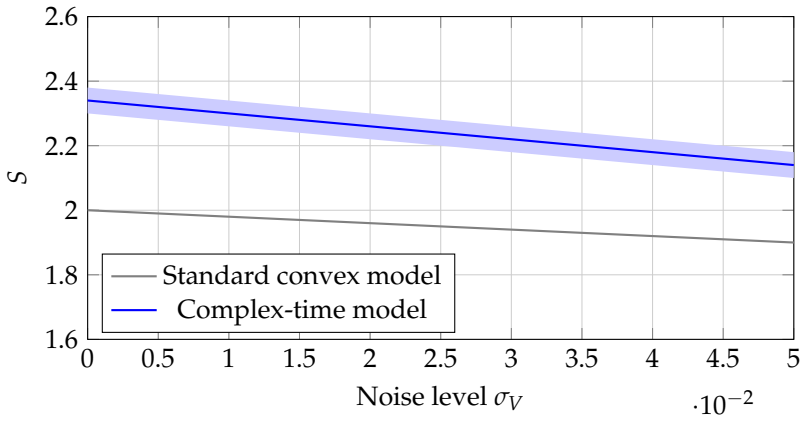

Figure 3. Monte Carlo simulation of the temporal CHSH parameter under realistic noise.

10. Perspectives and Future Implications

The complex-time framework developed in this work extends beyond the analysis of delayed-choice experiments. Its two-component temporal structure suggests several theoretical and experimental directions in which the internal geometry (t, τ) may play a role in the description of coherence and quantum dynamics.

10.1. Geometric Interpretation of Decoherence

In standard formulations, decoherence is modelled as an effective process arising from system–environment interactions, typically described by a Lindblad equation. While operationally successful, this approach does not specify a geometric mechanism underlying the attenuation of coherence. In the present framework, loss of visibility corresponds to a translation along the imaginary component of time,

$$\mathcal{V} = \exp(-\Gamma\,|\Delta\tau|), \qquad \Gamma = \Gamma_{\text{eff}}, \tag{85}$$

linking decoherence to an internal temporal structure rather than to an external environment. This perspective is consistent with geometric and internal-time approaches to quantum evolution [17–19,32] and may provide a basis for more predictive models of coherence loss in complex systems.

10.2. Internal Rotation as a Control Parameter

If coherence is encoded in the imaginary component τ, then the internal rotation angle θ constitutes a natural control parameter. Adjusting θ modifies τ and therefore the visibility. This idea is compatible with approaches in which generalised phases or internal variables play an operational role [33]. The internal temporal geometry may thus offer new tools for coherence control, qubit stabilisation, or interferometric protocols.

10.3. Relation to Retrocausal Models

Retrocausal interpretations [8,9] attempt to account for certain quantum correlations by allowing influences from future measurement settings. The complex-time model reproduces some of the operational features associated with such approaches, but without modifying the causal structure of real time: the dependence on the final configuration acts on the internal coordinate τ, not on t. This provides a geometric mechanism that avoids retrocausal dynamics while capturing similar operational effects.

10.4. Experimental Falsifiability

The temporal correlations defined by $C(x, y)$ allow one to construct a CHSH-type combination,

$$S = C(x_1, y_1) + C(x_1, y_2) + C(x_2, y_1) - C(x_2, y_2), \tag{86}$$

 doi:10.20944/preprints202602.1695.v1

whose classical bound $S_{\text{std}} \leq 2$ holds under the assumptions of one-dimensional convex and factorisable decoherence models. Any exceedance of this bound within the operational protocol considered here would indicate that coherence cannot be described by a purely real temporal dynamics. This places the complex-time model within the class of experimentally testable extensions of quantum theory, in the spirit of Bell-type analyses [10,11] and consistent-histories approaches [34–37].

10.5. Connection to Imaginary Time and Spacetime Geometry

Imaginary time appears in several areas of theoretical physics, including Wick rotations, Euclidean quantum gravity, and statistical mechanics. The present framework provides a minimal setting in which an imaginary temporal component acquires a geometric and operational meaning. The internal rotation of complex time may eventually be related to geometric or gravitational effects, offering a possible route toward a unified description of temporal structure in quantum theory.

In summary, the complex-time framework provides a geometric structure for coherence that is compatible with standard quantum mechanics while offering new avenues for theoretical development and experimental investigation. Its bidimensional temporal geometry may contribute to future progress in quantum control, decoherence modelling, and the conceptual foundations of quantum physics.

11. Conclusions

The complex-time framework developed in this work provides a geometric reparametrisation of coherence within standard quantum mechanics. The temporal variable

$$\mathcal{T} = t - i\tau, \tag{87}$$

defines a two-dimensional internal geometry in which the real component t governs causal evolution while the imaginary component τ parametrises the attenuation of coherence. The associated metric

$$ds^2_{\text{int}} = dt^2 + d\tau^2 = dR^2 + R^2 d\theta^2, \tag{88}$$

allows one to formulate an effective dynamics for τ through a variational principle, with the modulus R acting as a complex proper time invariant under internal rotations. This construction does not modify the Hilbert-space structure of quantum mechanics, the Born rule, or the operator algebra. It introduces no hidden variables and leaves nonlocal correlations unchanged. The imaginary component τ corresponds operationally to a local CP–TP dephasing channel and geometrically to a rotation in the internal temporal plane. Within this geometry, coherence depends on the imaginary-time difference

$$\mathcal{V} = \exp(-\Gamma_{\text{eff}}\,|\Delta\tau|), \tag{89}$$

and changes in the interferometric configuration correspond to rotations of complex time that modify $\Delta\tau$. This mechanism accounts for the dependence of visibility on late choices without altering the causal evolution in t, consistent with the operational structure observed in modern delayed-choice experiments [1,3,25,26]. Section 9 illustrated these effects numerically, showing exponential visibility decay, nonlinear dependence of $\Delta\tau$ on internal rotations, and temporal CHSH values that may exceed the classical bound under the convexity and factorisation assumptions of one-dimensional decoherence models. These results demonstrate that the framework yields quantitative and falsifiable predictions, consistent with recent analyses of temporal correlations and steering [12–15]. The complex-time model therefore provides a geometric and dynamical description of local coherence absent from the standard formalism, while preserving all nonlocal features of quantum mechanics. Its key empirical signature is the possibility of observing $S > 2$ in a visibility-based temporal CHSH protocol, which would indicate that coherence cannot be described by a purely real, one-dimensional temporal dynamics and would motivate a dedicated LGI/NSIT analysis [36,37].

 doi:10.20944/preprints202602.1695.v1

Supplementary Materials: The following supporting information can be downloaded at the website of this paper posted on Preprints.org. Supplementary Material S1: Monte Carlo procedure and analytical calculations supporting Section 8 of the main text.

Author Contributions: Conceptualization, G.R.; writing—original draft, G.R.; writing—review and editing, G.R. All authors have read and agreed to the published version of the manuscript.

Funding: This research received no external funding.

Institutional Review Board Statement: Not applicable.

Informed Consent Statement: Not applicable.

Data Availability Statement: No datasets were generated or analysed in this work.

Conflicts of Interest: The author declares no conflict of interest.

Abbreviations

The following abbreviations are used in this manuscript:

MDPI	Multidisciplinary Digital Publishing Institute
DOAJ	Directory of open access journals
TLA	Three letter acronym
LD	Linear dichroism

Appendix A. Possible Experimental Test of the Internal Temporal Structure

This appendix outlines an interferometric protocol that could test the physical relevance of the imaginary-time component τ introduced in the complex-time model. The aim is to compare the predictions of standard quantum mechanics—including classical environmental decoherence—with those of the internal temporal geometry.

Appendix A.1. Two Competing Descriptions

Consider a Mach–Zehnder interferometer fed with single photons. After the first beam splitter (BS1), the state is

$$|\psi\rangle = \frac{1}{\sqrt{2}}\big(|A\rangle + e^{i\phi}|B\rangle\big), \tag{A1}$$

with ϕ a controllable phase.

Standard model.

Each path interacts differently with an environment E:

$$|A\rangle|e_0\rangle \to |A\rangle|e_A\rangle, \qquad |B\rangle|e_0\rangle \to |B\rangle|e_B\rangle, \tag{A2}$$

yielding the visibility

$$\mathcal{V}_{\text{std}} = |\langle e_A|e_B\rangle|. \tag{A3}$$

Complex-time model.

The accumulated phase is parametrised by $\mathcal{T} = t - i\tau$, giving

$$\mathcal{V}_{\text{cplx}} = \exp(-\Gamma_{\text{eff}}\,|\Delta\tau|). \tag{A4}$$

Appendix A.2. Interferometer with Two Delayed Choices

We consider two independent late choices:

- a setting $x \in \{x_1, x_2\}$ modifying one arm (phase shifter, EOM, or controlled dephasing);
- a setting $y \in \{y_1, y_2\}$ modifying the final recombination (presence of BS2 or additional phase).

 doi:10.20944/preprints202602.1695.v1

Both choices are made after BS1 and can be causally separated using long fibres and fast modulators, as in modern delayed-choice experiments [1,3,25,26]. For each pair (x, y), the visibility $\mathcal{V}(x, y)$ is measured.

Appendix A.3. Standard Visibility Structure

In the standard model,

$$\mathcal{V}_{\text{std}}(x, y) = |\langle e_A(x, y)|e_B(x, y)\rangle|, \tag{A5}$$

implying:

- $0 \leq \mathcal{V}_{\text{std}} \leq 1$,
- monotonic decay under increasing noise,
- convexity under statistical mixing.

Appendix A.4. Complex-Time Model and Temporal Correlations

In the complex-time model,

$$\mathcal{V}_{\text{cplx}}(x, y) = \exp[-\Gamma_{\text{eff}}|\Delta\tau(x, y)|]. \tag{A6}$$

Define the temporal correlation

$$C(x, y) = 2\mathcal{V}(x, y) - 1, \tag{A7}$$

and the CHSH-type combination

$$S = C(x_1, y_1) + C(x_1, y_2) + C(x_2, y_1) - C(x_2, y_2). \tag{A8}$$

Classical one-dimensional temporal models satisfying macrorealism and non-invasive measurability obey the Leggett–Garg bound [38] and, more generally, the temporal CHSH bound $|S| \leq 2$ [39,40]. The bidimensional internal temporal structure introduced by the complex-time model departs from these assumptions and allows, in principle, values $S > 2$ within the same operational protocol, consistent with recent analyses of temporal correlations and steering [12–15].

Appendix A.5. Experimental Orders of Magnitude

Amplitude of τ.

For a visible photon ($E \simeq 1$ eV),

$$|\Delta\tau| \sim \frac{\hbar}{E}|\ln \mathcal{V}| \sim 3 \times 10^{-17}\,\text{s}. \tag{A9}$$

Values

$$R \sim 10^{-16}\text{–}10^{-15}\,\text{s} \tag{A10}$$

are sufficient for measurable variations.

Visibility precision.

Fibre interferometers routinely achieve

$$\delta\mathcal{V} \sim 10^{-3}\text{–}10^{-2}. \tag{A11}$$

Control elements.

- EOM: $f_{\text{EOM}} \sim$ 1–10 GHz, $\Delta t_{\text{switch}} \sim 10^{-10}$–$10^{-9}$ s;
- fibres: $L \sim$ 100 m–1 km, $\Delta t_{\text{fib}} \sim$ 0.5–5 μs;
- fast controllers: $\Delta t_{\text{ctrl}} \sim$ 1–10 ns.

These orders of magnitude indicate that:

 doi:10.20944/preprints202602.1695.v1

1. variations of τ of order 10^{-17}–10^{-16} s are detectable;
2. causally separated delayed choices are feasible with current technology;
3. the required values of R are compatible with experimental exploration.

Appendix A.6. CHSH Bound in a Standard Model

In a one-dimensional time model,

$$\mathcal{V}_{\text{std}}(x,y) = \int d\lambda\, p(\lambda)\, v(x,y,\lambda), \qquad v \in [0,1]. \tag{A12}$$

Setting $c = 2v - 1 \in [-1,1]$, the combination

$$S(\lambda) = c_{11} + c_{12} + c_{21} - c_{22} \tag{A13}$$

satisfies $|S(\lambda)| \leq 2$, hence

$$|S_{\text{std}}| \leq 2. \tag{A14}$$

In the complex-time model,

$$\mathcal{V}(x,y) = \exp[-\Gamma_{\text{eff}}|\Delta\tau(x,y)|], \tag{A15}$$

nonlinear dependencies of $\Delta\tau$ allow values $S > 2$, indicating that real-time evolution alone cannot capture the full structure of coherence.

References

1. Peruzzo, A.; Shadbolt, P.; Brunner, N.; Popescu, S.; O'Brien, J.L. A Quantum Delayed-Choice Experiment. *Science* **2012**, *338*, 634–637. https://doi.org/10.1126/science.1226719.
2. Kaiser, F.; Coudreau, T.; Milman, P.; Ostrowsky, D.B.; Tanzilli, S. Entanglement-Enabled Delayed-Choice Experiment. *Science* **2012**, *338*, 637–640. https://doi.org/10.1126/science.1226755.
3. Ma, X.S.; Kofler, J.; Zeilinger, A. Delayed-Choice Gedanken Experiments and Their Realizations. *PNAS* **2013**, *110*, 1221–1226. https://doi.org/10.1073/pnas.1213201110.
4. Manning, A.G.; Khakimov, R.I.; Dall, R.G.; Truscott, A.G. Wheeler's Delayed-Choice Experiment with a Single Atom. *Nat. Phys.* **2015**, *11*, 539–542. https://doi.org/10.1038/nphys3343.
5. Wheeler, J.A. The "Past" and the "Delayed-Choice" Double-Slit Experiment. In *Mathematical Foundations of Quantum Theory*; Marlow, A.R., Ed.; Academic Press: New York, 1978; pp. 9–48.
6. Wheeler, J.A. Law Without Law. In *Quantum Theory and Measurement*; Wheeler, J.A.; Zurek, W.H., Eds.; Princeton Univ. Press: Princeton, 1984; pp. 182–213.
7. Aharonov, Y.; Vaidman, L. Properties of a Quantum System During the Time Interval Between Two Measurements. *Phys. Rev. A* **1990**, *41*, 11–20. https://doi.org/10.1103/PhysRevA.41.11.
8. Price, H. *Time's Arrow and Archimedes' Point: New Directions for the Physics of Time*; Oxford University Press: Oxford, 1996.
9. Wharton, K. Time-Symmetric Quantum Mechanics. *Found. Phys.* **2010**, *40*, 313–332. https://doi.org/10.1007/s10701-009-9387-9.
10. Aspect, A.; Grangier, P.; Roger, G. Experimental Realization of Einstein-Podolsky-Rosen-Bohm Gedanken-experiment: A New Violation of Bell's Inequalities. *Phys. Rev. Lett.* **1982**, *49*, 91–94. https://doi.org/10.1103/PhysRevLett.49.91.
11. Aspect, A.; Dalibard, J.; Roger, G. Experimental Test of Bell's Inequalities Using Time-Varying Analyzers. *Phys. Rev. Lett.* **1982**, *49*, 1804–1807. https://doi.org/10.1103/PhysRevLett.49.1804.
12. Fritz, T. Quantum Correlations in the Temporal CHSH Scenario. *New J. Phys.* **2010**, *12*, 083055. https://doi.org/10.1088/1367-2630/12/8/083055.
13. Quintino, M.T.; Uola, R.; Budroni, C.; Gühne, O. Inequivalence of temporal and spatial quantum correlations. *Phys. Rev. Lett.* **2019**, *123*, 180401. https://doi.org/10.1103/PhysRevLett.123.180401.
14. Uola, R.; Costa, A.C.S.; Nguyen, H.C.; Gühne, O. Quantum Steering in Temporal Scenarios. *Phys. Rev. A* **2018**, *98*, 050102. https://doi.org/10.1103/PhysRevA.98.050102.
15. Chen, S.L.; Li, C.M.; Chen, N.L.; Lambert, N.; Nori, F. Temporal steering inequality. *Physical Review A* **2014**, *90*, 032115. https://doi.org/10.1103/PhysRevA.90.032115.

 doi:10.20944/preprints202602.1695.v1

16. Clauser, J.F.; Horne, M.A.; Shimony, A.; Holt, R.A. Proposed Experiment to Test Local Hidden-Variable Theories. *Phys. Rev. Lett.* **1969**, *23*, 880–884. https://doi.org/10.1103/PhysRevLett.23.880.
17. Zurek, W.H. Decoherence, einselection, and the quantum origins of the classical. *Rev. Mod. Phys.* **2003**, *75*, 715–775. https://doi.org/10.1103/RevModPhys.75.715.
18. Mostafazadeh, A. Pseudo-Hermitian representation of quantum mechanics. *Int. J. Geom. Methods Mod. Phys.* **2010**, *7*, 1191–1306. https://doi.org/10.1142/S0219887810004816.
19. Garrison, J.C.; Wright, E.M. Complex time path integrals and quantum evolution. *Phys. Lett. A* **2012**, *376*, 1233–1237. https://doi.org/10.1016/j.physleta.2012.02.047.
20. Weinberg, S. *Lectures on Quantum Mechanics*, 2 ed.; Cambridge University Press: Cambridge, 2015.
21. Nakahara, M. *Geometry, Topology and Physics*, 2 ed.; Taylor & Francis, 2003.
22. Frankel, T. *The Geometry of Physics: An Introduction*, 3 ed.; Cambridge University Press: Cambridge, 2011.
23. Simon, B. Holonomy, the quantum adiabatic theorem, and Berry's phase. *Physical Review Letters* **1983**, *51*, 2167–2170.
24. Berry, M.V. Quantal phase factors accompanying adiabatic changes. *Proceedings of the Royal Society A* **1984**, *392*, 45–57.
25. Vedovato, F.; Agnesi, C.; Giustina, M.; et al. Extending Wheeler's delayed-choice experiment to space. *Phys. Rev. Lett.* **2017**, *118*, 230402. https://doi.org/10.1103/PhysRevLett.118.230402.
26. Kaiser, F.; Coudreau, T.; Milman, P.; Tanzilli, S. Quantum delayed-choice experiment with entanglement. *Sci. Adv.* **2020**, *6*, eaaz4204. https://doi.org/10.1126/sciadv.aaz4204.
27. Wick, G.C. Properties of Bethe-Salpeter Wave Functions. *Physical Review* **1954**, *96*, 1124–1134.
28. Schwinger, J. On gauge invariance and vacuum polarization. *Physical Review* **1951**, *82*, 664–679.
29. Feynman, R.P.; Hibbs, A.R. *Quantum Mechanics and Path Integrals*; McGraw–Hill: New York, 1965.
30. Gibbons, G.W.; Hawking, S.W. Action integrals and partition functions in quantum gravity. *Physical Review D* **1977**, *15*, 2752–2756.
31. Brukner, Č.; Zeilinger, A. Information and fundamental elements of the structure of quantum theory. *Found. Phys.* **2004**, *34*, 1741–1750. https://doi.org/10.1023/B:FOOP.0000049576.72717.a5.
32. Page, D.N.; Wootters, W.K. Evolution without Evolution: Dynamics Described by Stationary Observables. *Phys. Rev. D* **1983**, *27*, 2885–2892. https://doi.org/10.1103/PhysRevD.27.2885.
33. Aharonov, Y.; Albert, D.Z.; Vaidman, L. How the result of a measurement of a component of the spin of a spin-1/2 particle can turn out to be 100. *Phys. Rev. Lett.* **1988**, *60*, 1351–1354. https://doi.org/10.1103/PhysRevLett.60.1351.
34. Gell-Mann, M.; Hartle, J.B. Classical equations for quantum systems. *Phys. Rev. D* **1993**, *47*, 3345–3382. https://doi.org/10.1103/PhysRevD.47.3345.
35. Griffiths, R.B. Consistent histories and the interpretation of quantum mechanics. *J. Stat. Phys.* **1984**, *36*, 219–272. https://doi.org/10.1007/BF01015734.
36. Budroni, C.; Emary, C. Temporal Quantum Correlations and Leggett–Garg Inequalities in Multi-Level Systems. *Phys. Rev. Lett.* **2014**, *113*, 050401. https://doi.org/10.1103/PhysRevLett.113.050401.
37. Halliwell, J.J. Leggett–Garg inequalities and the temporal CHSH inequality. *Phys. Rev. A* **2016**, *93*, 022123. https://doi.org/10.1103/PhysRevA.93.022123.
38. Leggett, A.J.; Garg, A. Quantum mechanics versus macroscopic realism: Is the flux there when nobody looks? *Physical Review Letters* **1985**, *54*, 857–860.
39. Kofler, J.; Brukner, Č. Classical world arising out of quantum physics under the restriction of coarse-grained measurements. *Physical Review Letters* **2007**, *99*, 180403.
40. Emary, C.; Lambert, N.; Nori, F. Leggett–Garg Inequalities. *Rep. Prog. Phys.* **2014**, *77*, 016001. https://doi.org/10.1088/0034-4885/77/1/016001.